C. R. Physique 15 (2014) 151–157

Contents lists available at ScienceDirect

Comptes Rendus Physique

www.sciencedirect.com

Electron microscopy / Microscopie électronique

Elemental analysis down to the single atom with electron beams

Analyse élémentaire d'un atome individuel avec un faisceau d'électrons

Kazu Suenaga

Nanotube Research Center, National Institute of Advanced Industrial Science and Technology (AIST), Central 5, 1-1-1 Higashi, Tsukuba 305-8565, Japan

ARTICLE INFO

Article history:
Available online 27 January 2014

Keywords:
STEM
EELS
EDX
Single atom spectroscopy
Low-dimension materials

Mots-clés :
STEM
Spectroscopie de perte d'énergie
Analyse dispersive en énergie
Spectroscopie d'atome unique
Matériaux à basse dimension

ABSTRACT

Recently the possibilities of chemical analysis by means of electron energy-loss spectroscopy (EELS) and energy dispersive X-ray spectroscopy (EDX) have been pushed to the single atom limit. Here we show examples for successful single-atom spectroscopy in low-dimensional materials using scanning transmission electron microscopy (STEM) together with EELS and EDX.

RÉSUMÉ

Au cours des années récentes, les techniques d'analyse spectroscopique de perte d'énergie (EELS) et d'émission X (EDX) ont été poussées jusqu'à l'identification d'atomes individuels. Nous présentons ici une sélection de résultats récents acquis en microscopie électronique à balayage en transmission (STEM) équipée pour les spectroscopies EELS et EDX, qui montrent des succès enregistrés sur des atomes uniques au sein de matériaux de basse dimensionnalité.

Requirements to analyze the atomic structure of matter with high sensitivity and high precision are more and more crucial for cutting-edge researches. Elemental analysis down to the single atom limit was first demonstrated in the last century with a successful detection of Gd dopant atoms in carbon nano-peapods [1]. A fully digitized STEM–EELS system enabling the recording of image-spectra [2] was used for statistical data analysis. Specimen damage due to the high dose of the incident electron beam required to isolate the signals from individual atoms was an intrinsic problem in such highly delicate analysis. Single atom detection by means of EELS had been anticipated by Isaacson and Johnson [3]. But their assumption did not consider the atomic movements induced by the incident electron probe itself. A most important point for realizing single atom spectroscopy is in fact to prevent the atoms from being kicked out during observations. If the atoms were completely immobile under the electron probe, any measurement of single atom properties would be possible. In order to reduce the atomic movements and also to enhance the EELS contrast, a lower accelerating voltage is preferred for single atom detection. In this article, I would like to emphasize the advantages of the low voltage STEM on three points, namely (i) less knock-on probability, (ii) higher EELS/EDX contrast, and (iii) less pronounced delocalization effect.

In order to compensate the inferior spatial resolution associated with lower-voltage STEM, more sophisticated electron optics are definitely required to reduce the residual aberrations. Sawada et al. designed a new type of aberration corrector

E-mail address: suenaga-kazu@aist.go.jp.

1631-0705/$ – see front matter
http://dx.doi.org/10.1016/j.crhy.2013.12.003

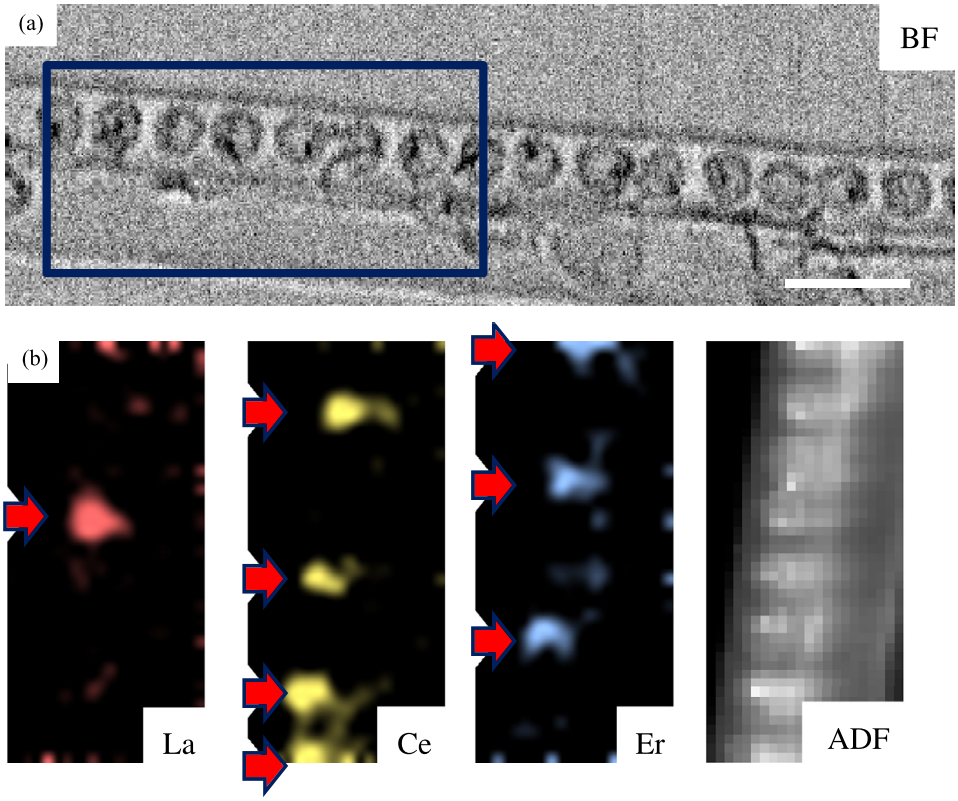

Fig. 1. (Color online.) "Labeling atom-by-atom" realized by means of STEM–EELS operated at 30 kV. (a) An area for the spectrum-imaging is shown in the BF image, which contains eight molecules either La@C_{82}, Ce@C_{82} or Er@C_{82}. (b) The La N-edge, Ce N-edge and Er N-edge have been extracted and used to construct the chemical maps for each. There are one La, four Ce and three Er atoms detected (indicated by red arrows). The simultaneously recorded ADF image is also shown. Scale bar = 2 nm. See also Ref. [10].

with triple dodecapole elements (DELTA system) to reduce the higher-order geometric astigmatism [4–6], which is very critical for the STEM performance operated at low accelerating voltages between 15 to 60 kV. One of the first examples of low-voltage STEM experiments has shown chemical analysis of individual molecules without massive structural destruction [7]. Higher-dose experiments, however, still show non-negligible irradiation damage on metallofullerene molecules, as proved by the escape of the encaged atoms even at 60 kV [8]. This problem has been anticipated, based on a simple calculation of the knock-on threshold energy [9]. The calculated knock-on threshold energies for the various carbon materials suggest that the accelerating voltage of 60 kV may not be low enough to completely avoid irradiation damage. An accelerating voltage below ∼35 kV is to be preferred for observing fullerene molecules [10]. Here we demonstrate single atom spectroscopy with hardly any irradiation damage realized by further reducing the accelerating voltage down to 30 kV. We have employed an electron energy-loss spectrometer dedicated for low-voltage operation (GIF Quantum, modified) [11].

Metallofullerene molecules encapsulated within a single-wall nanotube (SWNT), so-called peapod, were analyzed using a 30-kV operating voltage [10]. C_{82} molecules were chosen and co-doped with rare earth elements La, Ce, or Er inside the SWNTs. We denote such structures as M@C_{82} where M = La, Ce, or Er. The results are shown in Fig. 1. A BF image clearly shows the aligned molecular structures encapsulated inside the SWNT (Fig. 1(a)). In the indicated rectangular area, eight metallofullerene molecules are involved and each of them carries one metal atom, appearing in darker contrast, inside the caged structure. As the BF image does not bring us any elemental information of these eight molecules, we must identify these atoms by EELS chemical analysis. Fig. 1(b) shows EELS chemical maps obtained from the rectangle area in Fig. 1(a). The spectrum-image involving the La N-edge, Ce N-edge and Er N-edge was obtained with an acquisition time of 0.05 s for each EELS spectrum. The resulting signal to noise ratio is high enough to isolate the N-edges of individual atoms. The EELS chemical maps clearly discriminate the metal atoms and identify the chemical component for each molecule. We successfully identify three elements (La: $Z = 57$, Ce: $Z = 58$ and Er: $Z = 68$) as shown in Fig. 1(b).

Such analysis of metal atoms in peapods is rather simple because the distance between the metal atoms is large enough (∼1 nm) compared to the typical electron probe size and to the EELS signal delocalization effect (this term roughly designs the extent of the impact parameter between the incident electron and the center of the atom for producing the electron excitation at the origin of the EELS signal). A more challenging situation is to identify individual atoms in crystal structures where the adjacent atoms are closer to each other (typically 0.1 to 0.3 nm).

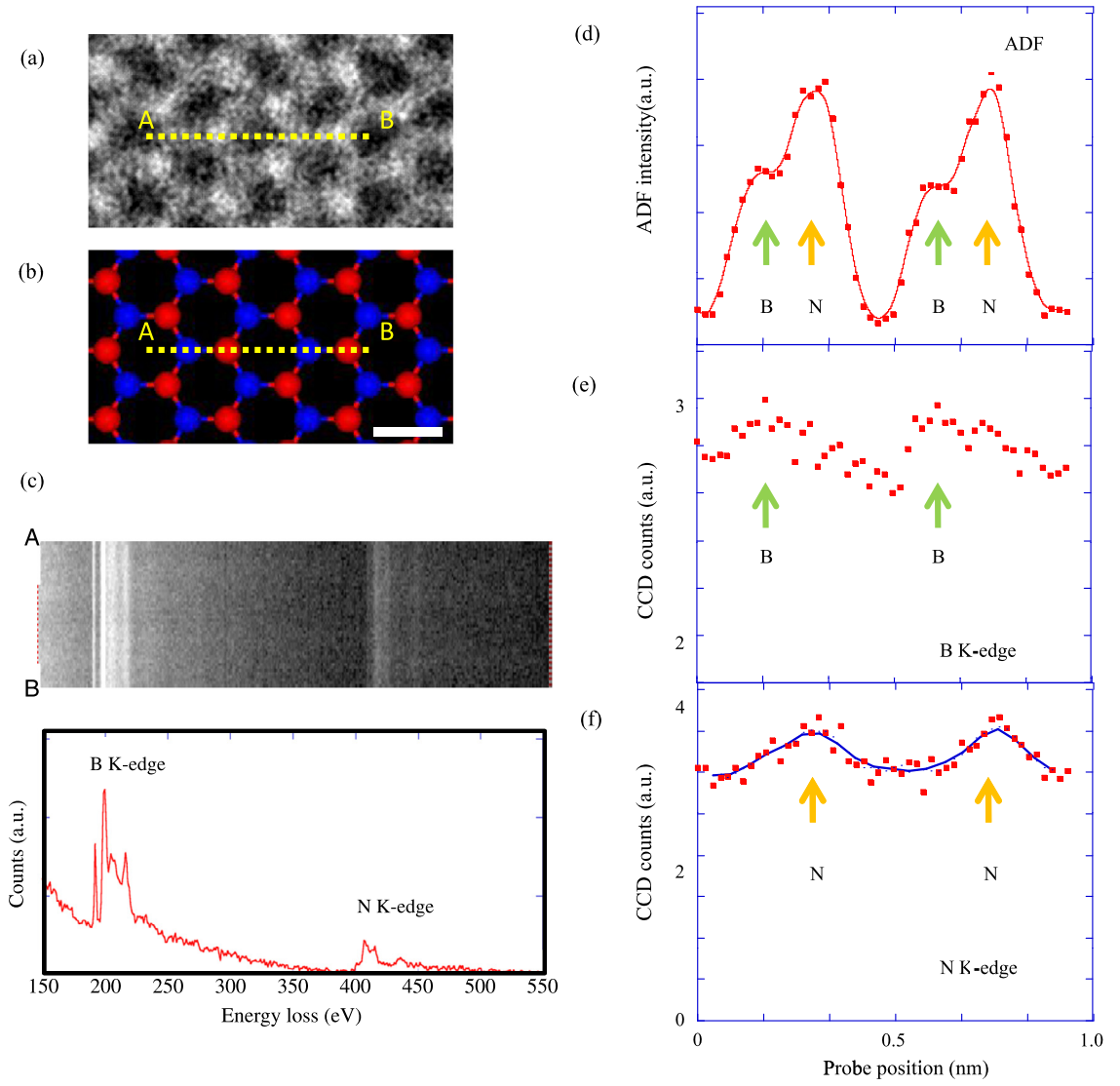

Fig. 2. (Color online.) (a), (b) An ADF image of single layered h-BN region that is free from structural defect and its corresponding atomic model where a line-spectrum has been recorded (indicated by a yellow line from A to B). A series of 50 spectra have been recorded with a step size of ∼0.02 nm. Each spectrum is acquired in 0.2 s. (c) A typical EELS spectrum (a sum of four) is shown and reflects the normal sp^2 bonded h-BN structure, involving the sharp π^* and σ^* for both B and N K-edges commonly observed. The convergent and collection angle for the EELS were 30 and 45–48 mrad, respectively. (d), (e), (f) Profiles for intensities of ADF, boron K-edge and nitrogen K-edge recorded along the yellow line in (a), (b). The ADF profile clearly reveals the B and N atomic positions. The nitrogen K-edge intensity shows the local maxima coincides to the N atomic positions while the boron K-edge shows a similar local maxima but much flat distribution due to the possible EELS signal delocalization. Principal component analysis (PCA) was performed to extract the boron K-edge profile. See Ref. [15].

Atomic assignments of single-layer hexagonal boron-nitride (h-BN) were performed by means of HR–TEM and STEM–ADF images [12–14]. The image contrast in both methods is attributed to the scattering ability difference between boron (B: $Z = 5$) and nitrogen (N: $Z = 7$). In order to unambiguously identify the atomic constituents, chemical analysis by means of EELS line-scan is performed on single-layer h-BN [15]. Fig. 2(a) and (b) show the ADF image and the corresponding atomic model where the line-scan was recorded. The probe was scanned across A to B along the yellow line in Fig. 2(a). Since the specimen is very fragile and is easily damaged during the spectrum-image, the experiment must be done with the minimum dose of electron beam.

Fig. 2(d), (e) and (f) show the intensity profiles of the ADF, boron K-edge and nitrogen K-edge signals. Four local maxima in the ADF profile correspond to the atomic positions of two boron and two nitrogen atoms. Because the ADF signals monotonically increase with atomic number (Z), the higher maxima in the ADF profile supposedly correspond to the nitrogen atomic positions and the lower maxima to the boron ones. This is confirmed by the nitrogen K-edge profile which shows two maxima indeed coinciding with the higher maxima in ADF profile. However, one can easily notice that the nitrogen K-edge intensity does not go down to zero even between two nitrogen atoms where no nitrogen atom exists. This is also

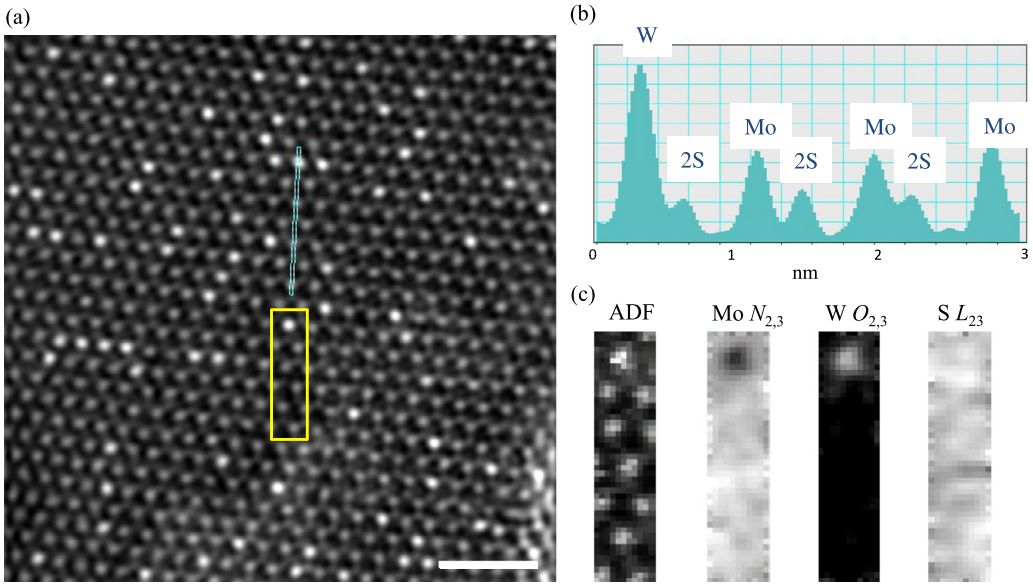

Fig. 3. (Color online.) (a) An ADF image of $Mo_{1-x}W_xS_2$ single layer with $x = 0.2$ (filtered), in which the atomic positions of sulfur are also visible. (b) Profile of the experimental ADF counts along the line indicated in (a). It confirms the W, Mo, and 2S atomic sites, i.e., the brighter spots correspond to W and the less bright ones to Mo. (c) Annular dark-field (ADF) image shows the rectangular region (yellow in (a)) over which a spectrum image was recorded. EELS chemical maps of Mo and W obtained simultaneously with the ADF image from the rectangle in (a). The energy dispersion was set to 0.25 eV with a binning of 2. The acquisition time for each spectrum is ∼0.05 s. The W O-edge and Mo N-edge were extracted after a background subtraction. They clearly show one W atom corresponding to the position with highest intensity in the ADF image of the rectangular area. Because the two edges are overlapping, the multiple linear least-squares fitting was performed on the low-loss spectra. Note that the spectra should be carefully recorded from the single layer regions without any carbon contamination. PCA was used to extract the chemical maps. Scale bar = 2 nm. See Ref. [18].

seen in the line-spectrum contrast in Fig. 2(f) and then a clear proof that the nitrogen profile is affected by the EELS signal delocalization. The large probe tail and mechanical instabilities such as the specimen drift during the line scan may also partly contribute to the non-zero intensity but this should not be dominant because the simultaneously recorded ADF profile clearly shows well-separated atoms.

The profile of the boron K-edge shows similar maxima at the boron atomic positions in the ADF profile, but these maxima are less pronounced in comparison with the nitrogen profile. The boron K-edge shows only a few percent difference in its intensity when the probe is on and off the boron atoms, while it is around 25% for the nitrogen K-edge. This different behavior in the profiles of the boron and nitrogen K-edges can be attributed to the energy-loss dependence of EELS signal delocalization. The delocalization is supposed larger at the boron K-edge (∼200 eV) than at the nitrogen K-edge (∼400 eV) by a factor of two [15]. It is therefore more difficult to see the local maxima in the boron K-edge profile rather than the nitrogen profile. Despite the inevitable delocalization effect, we are able to discriminate constituent atoms in the h-BN single layer which atomic distance is 0.14 nm apart.

Once the structures in 2D crystals were successfully assigned atom-by-atom, one can anticipate that more elaborate objectives can be targeted at the atomic scale. For example, doping, defects, alloying, and phase transition are all important phenomena in materials but have been mostly examined in a macroscopic viewpoint so far. Here we show an example to visualize how different atoms are mixed in a 2D alloy.

MoS_2 single layer shows interesting electronic and optical properties [16]. When MoS_2 is mixed with WS_2, the alloyed $Mo_{1-x}W_xS_2$ single layer can show a tunable bandgap [17]. STEM–ADF analysis is therefore instrumental to investigate how such a 2D alloy mixes distinct metal atoms [18]. Fig. 3 displays an ADF image of $Mo_{1-x}W_xS_2$ single layer with $x = 0.2$. The brighter contrast corresponds to W atom and less bright one to Mo atom as shown in Fig. 3(b). Quantitative analysis, which counts the number of hetero/homo adjacent atomic sites, clearly pleads for a random alloying behavior [18]. As shown in Fig. 3(c), EELS chemical mapping is attempted to identify the elements in a $Mo_{1-x}W_xS_2$ single-layer. Because the available edges of Mo and W are in the low-loss region, a multiple linear least square fitting was performed to extract the intensities of two edges. Reference spectra from pure MoS_2 and WS_2 single layers are both needed for the analysis. While the W O-edge map clearly shows a local maximum which corresponds to a W atom, the Mo N- and S L-edges do not exhibit atomic resolution. This is again the effect of EELS signal delocalization which is quite influential in this low-loss energy region (20 to 160 eV).

The physical properties of a graphene monolayer of finite lateral size are known to be governed by the edge structures and therefore understanding the edge properties is of great importance towards device applications of graphene. The electronic states of edges can be experimentally investigated with atomic resolution by means of EELS fine structures. The extremely weak signal and the intrinsic problem of specimen damage are the major obstacles for single atom spectroscopy of carbon displaying fine structure information. Despite the anticipated delocalization effect, discrimination of the single,

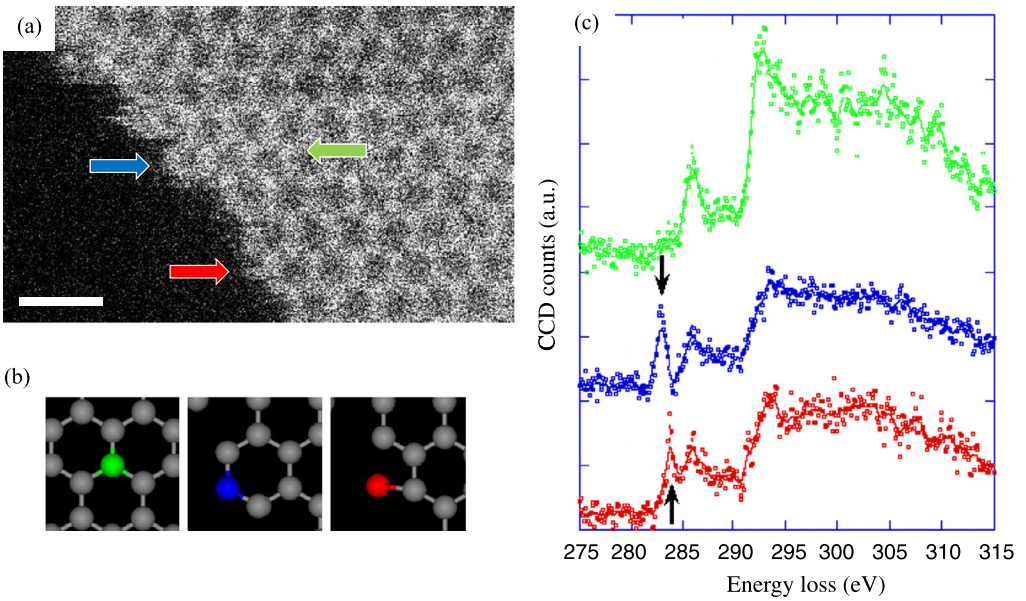

Fig. 4. Atom-by-atom spectroscopy at graphene edge. (a) STEM ADF image of a graphene edge region. (b) Different atomic configurations for each carbon atom painted in green (triple coordination), blue (double coordination) and red (single coordination). (c) Electron energy loss spectra from single carbon atoms with different coordination numbers [19]. For interpretation of references to color, see the online version of this article.

double and triple-coordinated carbon atoms at the graphene edge has been successfully demonstrated with atomic resolution (Fig. 4). Then peculiar electronic/bonding structures attributed to the graphene edge can be directly investigated through the site specific single-atom spectroscopy at the graphene edge. Our results demonstrate how rich information can be obtained from single atoms through the EELS fine structure analysis, which will open up a huge possibility to explore the local electronic structures of nano-scale devices and/or individual molecules.

The single atom detection by means of EDX has for long been considered more difficult because the photoemission rate is strongly reduced by the fluorescence yield. Furthermore, the detection efficiency for an X-ray photon in a STEM is generally quite low because of the limitation in the effective solid angle. A JEM–ARM200F microscope equipped with a large area silicon drift detector (SDD) was operated at 60 kV (Fig. 5(a)). Er@C_{82} peapods were used for the single atom EDX experiment. Er is also detectable by EELS, therefore direct comparison of the detection efficiency between EDX and EELS becomes possible. Since the simultaneous EELS acquisition can allow us to count the number of inelastic events, the fluorescence yield of single Er atoms can be directly estimated by a ratio of EDX and EELS intensities. Fig. 5(b) inset shows an ADF image of the examined metallofullerene peapods. Each brighter spot corresponds to a single Er atom positioned at regular intervals. The yellow dotted line shows where the incident electron probe scans across an Er atom (from up to down). Eighty pairs of EDX and EELS spectra were simultaneously acquired at constant increments along the line. The acquisition time for each probe position is 0.5 s. Fig. 5(b), (c) show EDX and EELS spectra extracted from the line-scan. Ten spectra are summed for each figure. The EDX spectrum clearly shows the peaks of Er M-line and Er L_α-line (indicated by the solid arrows) at 1.4 keV and 6.9 keV, respectively. The number of counted photons is around 10 counts for Er M and L-lines. Note that the counts do not increase monotonically even when the acquisition time is extended. This means that the Er atom is not completely immobile during the acquisition and that it can often be kicked out under the intense electron beam. Simultaneously recorded EELS spectra unambiguously show the Er N-edge (Fig. 5(c)). The S/N ratio is sufficiently quite high to identify and measure the EELS edge recorded with the same acquisition time as for EDX. If we compare the counting statistics, the EELS N-edge shows more than 5×10^5 electron counts for the N-edge after the standard background subtraction, while the EDX has only 10 to 20 photon counts for the L or M lines. Single atom detection by means of EDX is extremely disadvantageous in comparison with the EELS by four to five orders of magnitude in terms of the signal counts.

In both cases of EELS and EDX, inelastic events which are generated by the excitation of core electrons are counted. There is a clear difference in the counting efficiency between EELS and EDX. While transmission EELS can collect most of the forward-scattered electrons which suffers the specific energy-loss, EDX collects only the photons that are emitted towards the detector. Because the probability of photon emission is completely isotropic irrespective to the incident e-beam direction, the detection efficiency is definitely less than 1. In this experiment the detection efficiency is calculated to be 0.8 $\mathrm{sr}/4\pi$. Also the fluorescence yield is estimated as 10^{-3} to 10^{-4} for M-line photoemission. These numbers lead to the 4 or 5 orders of magnitude disadvantageous EDX for single atom detection. With a smaller detecting window, it takes more time to obtain the EDX signals from single atom [21].

In this short review, single atom spectroscopy by means of EELS and EDX is demonstrated to discriminate individual atoms of different nature. It has remained a challenge for scientists to see and identify individual atoms since Dalton first

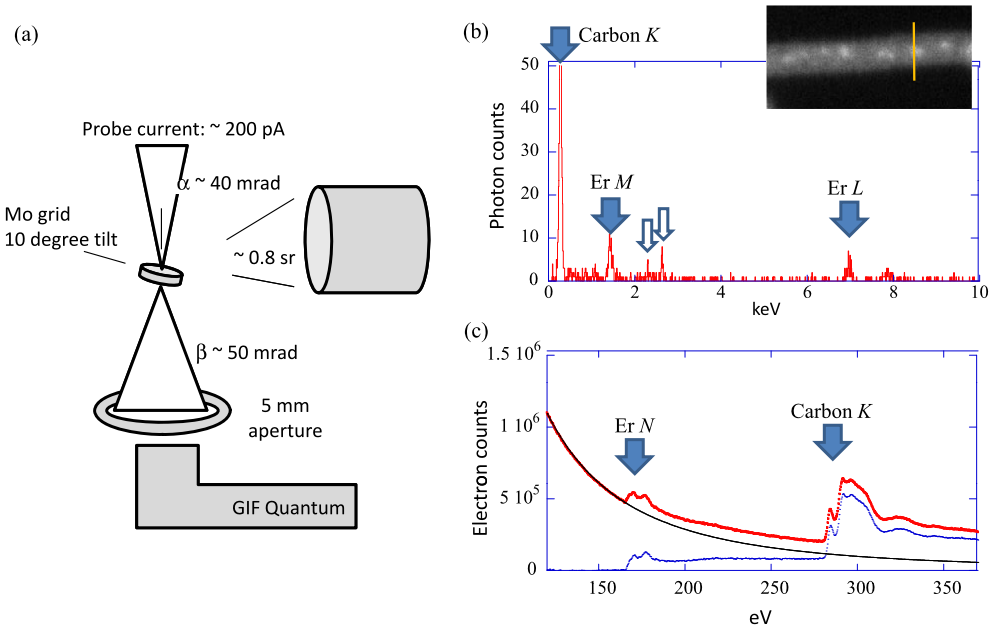

Fig. 5. (a) Experimental set up used for the simultaneous EDX and EELS chemical analyses [20]. The SDD is located at the side of the specimen with a solid angle (0.80 sr), while the EELS signal is recorded in transmission. (b) An ADF image of the specimen (inset). The brighter spots correspond to single Er atoms and are well distributed with a 1 nm interval on average. The yellow dotted line shows where a typical line-spectrum was recorded. (b) An EDX spectrum recorded from the line-scan. Er M and Er L lines are clearly visible as well as carbon K line (solid arrows). Open arrows show Mo, S, and Cl signals due to the Mo grid or the solvent used for the specimen preparation (carbon disulfide and hydrochloric acid). (c) An EELS spectrum recorded simultaneously with the EDX spectrum above. The Er N-edge shows a very high S/N ratio. For interpretation of references to color, see the online version of this article.

proposed distinct atoms in his atomic theory [22]. It is also clear that information on the bonding/electronic states has become accessible for single atoms through the EELS fine-structure analysis. Such analysis was not possible until recently because of two intrinsic limitations, namely, the inevitable irradiation damage due to the huge number of electrons required to realize a high enough signal-to-noise ratio for fine-structure analysis from a single atom, and the non-negligible EELS signal delocalization, which may affect the spatial resolution. Lowering the accelerating voltage could be the only way to overcome these two drawbacks.

Acknowledgements

This work was supported by JST–CREST and Research Acceleration programs.

References

[1] K. Suenaga, M. Tencé, C. Mory, C. Colliex, H. Kato, T. Okazaki, H. Shinohara, K. Hirahara, S. Bandow, S. Iijima, Element-selective single atom imaging, Science 290 (2000) 2280–2282.
[2] M. Tencé, M. Quartuccio, C. Colliex, PEELS compositional profiling and mapping at nanometer spatial resolution, Ultramicroscopy 58 (1995) 42–54.
[3] M. Isaacson, D. Johnson, The microanalysis of light elements using transmitted energy loss electrons, Ultramicroscopy 1 (1975) 33–52.
[4] H. Sawada, T. Sasaki, F. Hosokawa, S. Yuasa, M. Terao, M. Kawazoe, T. Nakamichi, T. Kaneyama, Y. Kondo, K. Kimoto, K. Suenaga, Correction of higher-order geometrical aberration by triple 3-fold astigmatism field, J. Electron Microsc. 58 (2009) 341–347.
[5] H. Sawada, T. Sasaki, F. Hosokawa, S. Yuasa, M. Terao, M. Kawazoe, T. Nakamichi, T. Kaneyama, Y. Kondo, K. Kimoto, K. Suenaga, Higher-order aberration corrector for an image-forming system in a transmission electron microscope, Ultramicroscopy 110 (2010) 958–961.
[6] T. Sasaki, H. Sawada, F. Hosokawa, Y. Kohno, T. Tomita, T. Kanayama, Y. Kondo, K. Kimoto, Y. Sato, K. Suenaga, Performance of low-voltage STEM/TEM with delta corrector and cold field emission gun, J. Electron Microsc. 59 (2010) S7–S13 (Supplement).
[7] K. Suenaga, Y. Sato, Z. Liu, H. Kataura, T. Okazaki, K. Kimoto, H. Sawada, T. Sasaki, K. Omoto, T. Tomita, T. Kaneyama, Y. Kondo, Visualizing and identifying single atoms using electron energy-loss spectroscopy with low accelerating voltage, Nat. Chem. 1 (2009) 415–418.
[8] O.L. Krivanek, N. Dellby, M.F. Murfitt, M.F. Chisholm, T.J. Penniyook, K. Suenaga, V. Nicolosi, Gentle STEM: ADF imaging and EELS at low primary energies, Ultramicroscopy 110 (2010) 935–945.
[9] F. Banhart, Irradiation effects in carbon nanostructures, Rep. Prog. Phys. 62 (1999) 1181–1221.
[10] K. Suenaga, Y. Iizumi, T. Okazaki, Single atom spectroscopy with reduced delocalization effect using a 30 kV STEM, Eur. Phys. J. Appl. Phys. 54 (2011) 33508.
[11] A. Gubbens, M. Barfels, C. Trevor, R. Twesten, P. Mooney, P. Thomas, N. Menon, B. Kraus, C. Mao, B. McGinn, The GIF Quantum, a next generation post-column imaging filter, Ultramicroscopy 110 (2010) 962–970.
[12] C. Jin, F. Lin, K. Suenaga, S. Iijima, Fabrication of a free-standing boron nitride single layer and its defects assignments, Phys. Rev. Lett. 102 (2009) 195505.
[13] O.L. Krivanek, M.F. Chisholm, V. Nicolosi, T.J. Pennycook, G.J. Corbin, N. Dellby, M.F. Murfitt, C.S. Own, Z.S. Szilagyi, M.P. Oxley, S.T. Pantelides, S.J. Pennycook, Atom-by-atom structural and chemical analysis by annular dark-field electron microscopy, Nature 464 (2010) 571–574.

[14] J.C. Meyer, S. Kurasch, H.J. Park, V. Skakalova, D. Künzel, A. Gross, A. Chuvilin, G. Algara-Siller, S. Roth, T. Iwasaki, U. Starke, J.H. Smet, U. Kaiser, Experimental analysis of charge redistribution due to chemical bonding by high-resolution transmission electron microscopy, Nat. Mater. 10 (2011) 209–215.
[15] K. Suenaga, H. Kobayashi, M. Koshino, Core-level spectroscopy of point defects in single layer h-BN, Phys. Rev. Lett. 108 (2012) 075501.
[16] B. Radisavljevic, A. Radenovic, J. Brivio, V. Giacometti, A. Kis, Single-layer MoS_2 transistors, Nat. Nanotechnol. 6 (2011) 147–150.
[17] Y. Chen, J. Xi, D. Dumcenco, Z. Liu, K. Suenaga, D. Wang, Z. Shuai, Y.-S. Huang, L. Xie, Tunable band-gap photoluminescence from atomically thin transition-metal dichalcogenide alloys, ACS Nano 7 (2013) 4610–4616.
[18] D.O. Dumcenco, H. Kobayashi, Z. Liu, Y.-S. Huang, K. Suenaga, Visualization and quantification of transition metal atomic mixing in $Mo_{1-x}W_xS_2$ single layers, Nat. Commun. 4 (2013) 1351.
[19] K. Suenaga, M. Koshino, Atom-by-atom spectroscopy at graphene edge, Nature 468 (2010) 1088–1090.
[20] K. Suenaga, T. Okazaki, E. Okunishi, S. Matsumura, Detection of photons emitted from single Er atoms in energy-dispersive EDX spectroscopy, Nat. Photonics 6 (2012) 545–548.
[21] T.C. Lovejoy, Q.M. Ramasse, M. Falke, A. Kaeppel, R. Terborg, R. Zan, N. Dellby, O.L. Krivanek, Single atom identification by energy-dispersive X-ray spectroscopy, Appl. Phys. Lett. 100 (2012) 154101.
[22] J. Dalton, A New System of Chemical Philosophy, Strand, London, 1808, printed by S. Russell for R. Bickerstaff.